

Magnetization induced skyrmion dynamics of a spin-orbit-coupled spinor condensate under sinusoidally varying magnetic field

Arpana Saboo,^{1,*} Soumyadeep Halder,¹ Mithun Thudiyangal,² and Sonjoy Majumder^{1,†}

¹*Department of Physics, Indian Institute of Technology Kharagpur, Kharagpur, West Bengal 721302, India*

²*Department of Physics and Electronics, Christ University, Bengaluru, Karnataka 560029, India*

We theoretically explore the spin texture dynamics of a harmonically trapped spin-1 Bose-Einstein condensate with Rashba spin-orbit coupling and ferromagnetic spin-exchange interactions under a sinusoidally varying magnetic field along the x -direction. This interplay yields an intrinsic spin texture in the ground state, forming a linear chain of alternating skyrmions at the saddle points. Our study analyzes the spin-mixing dynamics for both a freely evolving and a controlled longitudinal magnetization. The spin-1 system exhibits the Einstein-de Hass effect for the first case, for which an exchange between the total orbital angular momentum and the spin angular momentum is observed, resulting in minimal oscillations about the initial position of the skyrmion chain. However, for the fixed magnetization dynamics, the skyrmion chain exhibits ample angular oscillations about the equilibrium position, with the temporary formation of new skyrmions and anti-skyrmions to facilitate the oscillatory motion. Keeping the magnetization constant, this contrast now stems from the exchange between the canonical and spin-dependent contribution to the orbital angular momentum. The variation in canonical angular momentum is linked to the angular oscillations, while the spin-dependent angular momentum accounts for the creation or annihilation of skyrmions. We confirm the presence of scissor mode excitations in the spin texture due to the angular skyrmion oscillations.

Spinor Bose gases [1–5] form a family of quantum fluids with non-trivial spin internal degrees of freedom, manifesting the interplay of magnetism [6] and superfluidity [7], both of which involves quantum phase coherence [8], long-range order [9], and symmetry breaking [10, 11]. These degenerate fluids are interesting in their own right as they could be investigated for the system properties and the interaction between atomic states, shedding light on a range of topics such as quantum phase transitions [12], non-equilibrium quantum dynamics [13, 14] and instabilities [15, 16], the role of symmetry and topology in quantum-ordered materials [17, 18], topological defects [19], spin dynamics [20, 21], etc.

The experimental realization of spin-orbit coupling (SOC) [22–29] in neutral atoms has broadened the impact of ultracold-atom research and has drawn new participants and perspective to this field. Spin-orbit (SO) coupled spin-1 BECs are particularly interesting to explore as they exhibit certain exotic quantum states with engrossing topological structure in their order parameter which includes vortex lattice [30–32], half-quantum vortex [24, 33, 34], supersolid stripe phase [35–37], solitons [38], skyrmions [39–41], among others. For this reason, the degenerate spinor condensates qualify as an enticing bridge between the physics of ultracold atoms and solid states.

One of the most fascinating outcomes of introducing SOC in spin-1 BECs is the emergence of skyrmion spin textures [42, 43]. Skyrmions are topologically protected spin configurations that resemble spin vortices [44], stabilized by the interplay of SOC and atomic interactions. These textures present a unique opportunity to study topological excitations in a controlled environment. Investigating skyrmion textures enhances our understanding of

topological phases of matter and quantum vortices [45], with potential applications in quantum computing [46], spintronics [47], Spin Hall effect [48, 49], and advanced materials [50]. The study of skyrmions in SO-coupled spin-1 BECs underscores the profound implications of topological and spin-orbit phenomena in quantum fluids, paving the way for significant advancements in both theoretical and applied physics [51–55]. Moreover, the interaction of the SO-coupled BECs with the external magnetic field yields the local spin texture of the system [56–58]. Recent studies indicate that in-plane varying magnetic fields can be used to synthetically create non-Abelian gauge fields, which may lead to exotic phenomena in spin-1 BECs such as skyrmion lattice formation as discussed in [19].

In this letter, we investigate the interaction of a spin-orbit coupled spin-1 condensate confined in a Quasi-2D harmonic trap, with a sinusoidally varying magnetic field along the x -direction. We consider a Quasi-2D spin-orbit coupled $F = 1$ spinor condensate of N atoms with mass M confined in an external axisymmetric potential $V(\mathbf{r})$ at zero temperature. In the mean-field theory, the effective Hamiltonian of the system is described by [59],

$$H_{2D} = \int d\mathbf{r} \left(\Psi^\dagger \left[-\frac{\hbar^2 \nabla^2}{2M} + V(\mathbf{r}) + \nu_{\text{soc}} + g_F \mu_B \mathbf{B}(\mathbf{r}) \cdot \mathbf{f} \right] \Psi + \frac{1}{2} g_0 n^2 + \frac{1}{2} g_2 |\mathbf{F}|^2 \right) \quad (1)$$

where $\Psi = [\Psi_1(\mathbf{r}), \Psi_0(\mathbf{r}), \Psi_{-1}(\mathbf{r})]^T$ with $\mathbf{r} = (x, y)$ is the spin-1 wave function where the three components describe the condensate amplitude in the spin levels $m_F = 1, 0, -1$, respectively, satisfying the normalization criteria, $\int d\mathbf{r} \Psi^\dagger \Psi = N$, with total atomic density $n = n_1 + n_0 + n_{-1} = \sum_{m_F} \Psi_{m_F}^\dagger \Psi_{m_F}$ and the spin density

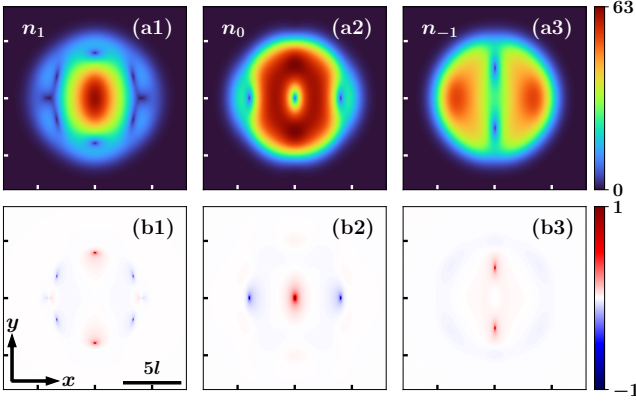


FIG. 1: (a1-a3) shows the ground state density profiles of a SO-coupled ferromagnetic spin-1 BEC of 10^4 ^{87}Rb atoms in a sinusoidally varying magnetic field $B(\mathbf{r}) = (B_0 \sin x, 0)$. The SOC strength $\gamma = 0.5\hbar\omega_\perp l$, $B_0 = 0.25\hbar\omega_\perp/g_F\mu_B l$. The scattering length $a_0 = 101.8a_B$ and $a_2 = 100.4a_B$. The spin-1 BEC is confined in an axisymmetric trap with $(\omega_\perp, \omega_z) = 2\pi \times (20, 400)\text{Hz}$. (b1-b3) shows the corresponding vorticity profiles which can be measured as $\Omega_{m_F} = \nabla \times \mathbf{J}_{m_F}$, with the probability current density $\mathbf{J}_{m_F} = \frac{i\hbar}{2M}(\psi_{m_F} \nabla \psi_{m_F}^* - \psi_{m_F}^* \nabla \psi_{m_F})$. The densities n_{m_F} expressed in units of l^{-2} where $l = 2.41\mu\text{m}$ is the characteristic length. The vorticity Ω_{m_F} is expressed in dimensionless units.

given as $|\mathbf{F}| = \Psi^\dagger \mathbf{F} \Psi$. Here, $\mathbf{F} = (F_x, F_y, F_z)$ represents the spin density vector defined as $F_\alpha = \Psi^\dagger f_\alpha \Psi$ ($\alpha = x, y, z$) with $\mathbf{f} = (f_x, f_y, f_z)$ being the irreducible representation of the 3×3 Pauli spin matrices and the longitudinal magnetization $m_z = \int d\mathbf{r} F_z(\mathbf{r})$. The spin-independent and spin-exchange interactions are characterized by g_0 and g_2 , respectively, corresponding to channels for which two colliding atoms have total spin 0, 2 respectively. $V(\mathbf{r}) = \frac{1}{2}M\omega_\perp^2(x^2 + y^2)$ is the Quasi-2D harmonic trap with ω_\perp being the radial trapping frequency and $l = \sqrt{\hbar/M\omega_\perp}$ being the harmonic oscillator length. The Rashba SOC interaction [22, 24] yields as $\nu_{\text{SOC}} = \gamma(f_x p_y - f_y p_x)$ where γ is the SOC strength and (p_x, p_y) represents the momentum in the quasi-2D space. $B(\mathbf{r}) = (B_0 \sin x, 0)$ is the externally applied magnetic field. Here, the Lande's g-factor $g_F = -\frac{1}{2}$ and μ_B is the Bohr magneton. In our study, we consider the effective B_0 to be negative.

We numerically solve the coupled Gross-Pitaevskii equations [see supplementary section S1 for details] to generate the ground state solutions of the spinor condensate with freely evolving longitudinal magnetization [60]. The spin-orbit coupling induces anisotropy in the system, leading to the rotational symmetry breaking. The combined effect of the external magnetic field and spin-orbit coupling results in density modulations in the system, materializing topological excitations in the form of vortices. In the ground state, we report the formation of a vortex

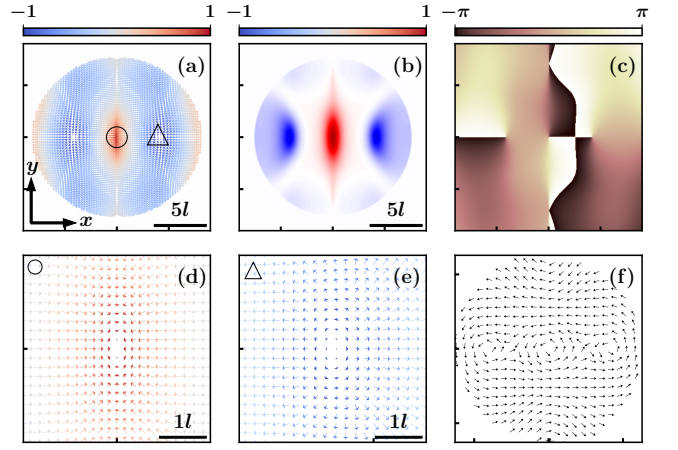


FIG. 2: (a) shows the spin texture \mathbf{S} of the initial state demonstrated in Fig. 1. The arrows represent the transverse (S_x, S_y) components, while the color of the arrows represents the magnitude of S_z . The skyrmion and anti-skyrmion are marked by a black circle and a black triangle, respectively. (b) shows the topological charge density of the equilibrium spin texture. (d) and (e) is the local amplification of the spin texture showing the skyrmion and anti-skyrmion structures, respectively. (c) shows the transverse spin-phase ϕ for the initial state and (f) shows the transverse spin velocity field, *i.e.*, $\vec{\nabla}\phi/|\vec{\nabla}\phi|$.

chain (at the saddle points of the magnetic field) in the $m_F = 0$ component density [see Fig. 1 (a2)]. The $m_F = 1$ component has a local high density at the center [see Fig. 1 (a1)], which is elongated along the y -axis with adjacent vortex-antivortex chains surrounding the local high density. The $m_F = -1$ component has vortices along the y -axis, with high-density lobes surrounding the axial line [see Fig. 1 (a3)]. The vorticity profile [see Fig. 1 (b1-b3)] clearly shows that the $m_F = 0$ component exhibits an alternating vortex-anti-vortex chain. Due to the induced anisotropy, the vortices have a slightly deformed elliptical core.

The interplay of the SOC and the external magnetic field yields a distinct arrangement of stable spin configurations (at the saddle points) described by the spin texture, $S_\alpha = \sum_{m_F, n_F} \psi_{m_F}^* (f_\alpha)_{m_F, n_F} \psi_{n_F} / \sum_{m_F} |\psi_{m_F}|^2$ ($\alpha = x, y, z$), $m_F, n_F = 0, \pm 1$ [61, 62]. In the ground state, we confirm a unique anti-skyrmion-skyrmion-anti-skyrmion chain as demonstrated in Fig. 2(a) [63]. In Fig. 2(b), we show the topological charge density, given as $q(\mathbf{r}) = \frac{1}{4\pi} \mathbf{s} \cdot \left(\frac{\partial \mathbf{s}}{\partial x} \times \frac{\partial \mathbf{s}}{\partial y} \right)$. Here $\mathbf{s} = \mathbf{S}/|\mathbf{S}|$, with $\mathbf{S} = (S_x, S_y, S_z)$. The associated topological charge Q is defined as $Q = \int q(\mathbf{r}) dx dy$. The local amplification of the skyrmion and anti-skyrmion structures are presented in Fig. 2(d) and Fig. 2(e), respectively. The spin phase $\phi = \arctan(S_y/S_x)$ is depicted in Fig. 2(c). The singularities in the spin phase denote the skyrmions in the

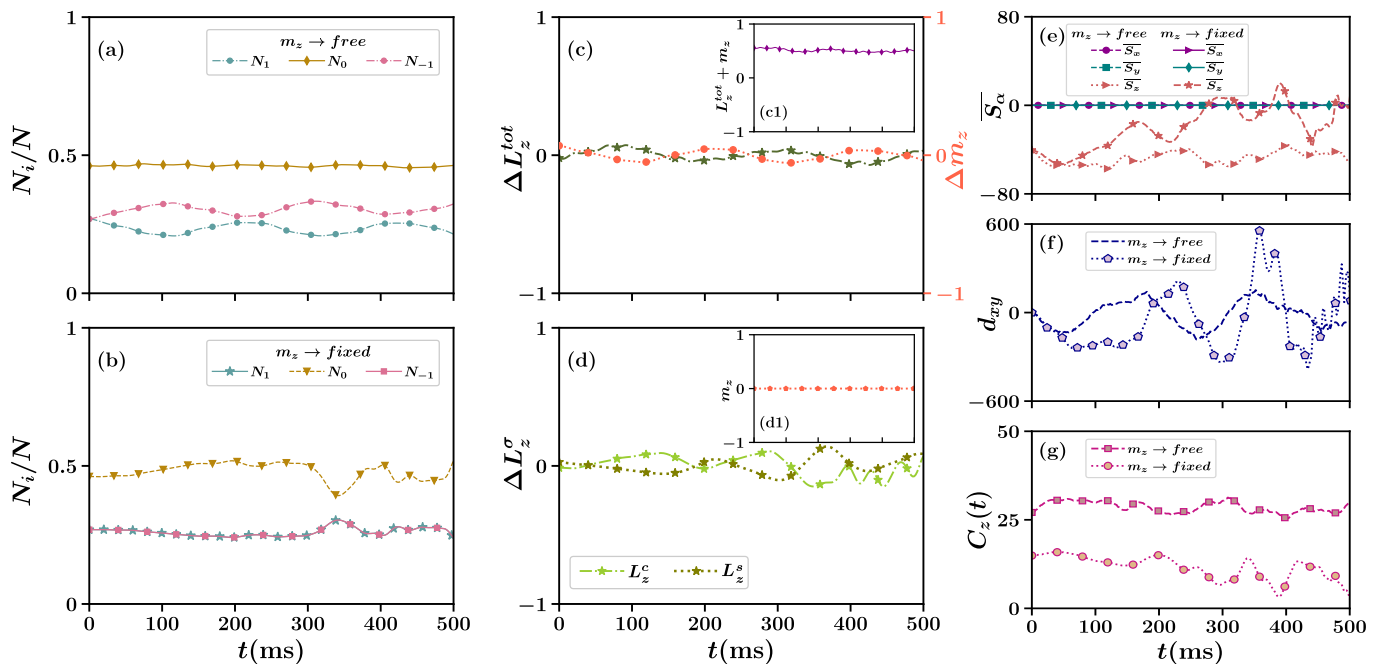


FIG. 3: (a) and (b) shows the component-wise particle number variation for the cases of skyrmion dynamics with freely evolving and fixed longitudinal magnetization; (c) represents the deviation of orbital angular momentum L_z^{tot} and spin angular momentum m_z from their average values [64] and the inset (c1) shows the total angular momentum for the free evolution; (d) shows the variation of the canonical and the spin-dependent term in the orbital angular momentum and the inset (d1) shows the m_z variation for fixed magnetization dynamics; (e) represents the variation of the spatial average $\overline{S_\alpha} = \int S_\alpha dxdy$ with time; (f) denotes the spin-scissors modes for both cases and (g) represents the spin-spin time correlations for both cases.

guise of spin vortices. Figure 2(f) gives their associated spin velocity field. The time evolution of this prepared ground state reveals steady-state dynamics, maintaining a constant total angular momentum, L_z^{tot} for the spin-orbit coupled Hamiltonian, expressed as [65, 66],

$$L_z^{tot} = x(p_y + \gamma f_x) - y(p_x - \gamma f_y) = L_z^c + L_z^s, \quad (2)$$

where $L_z^c = xp_y - yp_x$ is the canonical contribution, while $L_z^s = \gamma(xf_x + yf_y)$ is the spin-dependent term. Additionally, the number of particles in each component remains the same throughout the dynamics, thereby preserving the longitudinal magnetization m_z . As a matter of fact, the total angular momentum (orbital plus spin) is a conserved quantity for the steady state [see Fig. S4]. Building on our investigation of the ground state's steady-state dynamics, we now explore how initializing the system with a predefined longitudinal magnetization m_z influences its static and dynamic properties.

Spin texture dynamics of the SO-coupled spin-1 BEC: We prepare the initial state with fixed magnetization $m_z = 0$ [67]. The density profile for this state resembles the ground state [Fig. 1] for which the magnetization settles at $m_z = -0.07$. To understand the role of magnetization in spin texture dynamics, we then study the evolution of the system under two scenarios of spin-mixing dynamics: (a) with freely evolving magnetization $m_z \neq 0$

and (b) with fixed magnetization $m_z = 0$, which we delve into in the ensuing section.

Case-I - Free magnetization dynamics: After initializing the system with $m_z = 0$, we allow it to evolve freely. As shown in Fig. 3(a), the population of particles ($N_{\pm 1}$) for the $m_F = \pm 1$ components, oscillates periodically due to the combined effects of spin-mixing dynamics and the applied external magnetic field. This oscillation results in a periodic modulation of m_z , highlighting the Einstein-de Haas effect [65, 66, 68]. This effect illustrates how the alignment of spins mechanically affects the condensate, further driving the intricate interplay between spin and orbital angular momentum. Consequently, the system exhibits a characteristic exchange between the spin m_z and total orbital angular momentum L_z^{tot} [64], as illustrated in Fig. 3(c), with the total angular momentum depicted in the inset, Fig. 3(c1). Interestingly, the skyrmion structures maintain relatively stable configurations, experiencing only minimal angular oscillations throughout the relaxed dynamics—a dynamic sequence provided in full in the supplementary materials.

Case-II- Fixed magnetization dynamics: Here, we keep m_z fixed even during the dynamics. To achieve this, we normalize the system after each step during the real-time propagation. With $m_z = 0$, the canonical and spin-

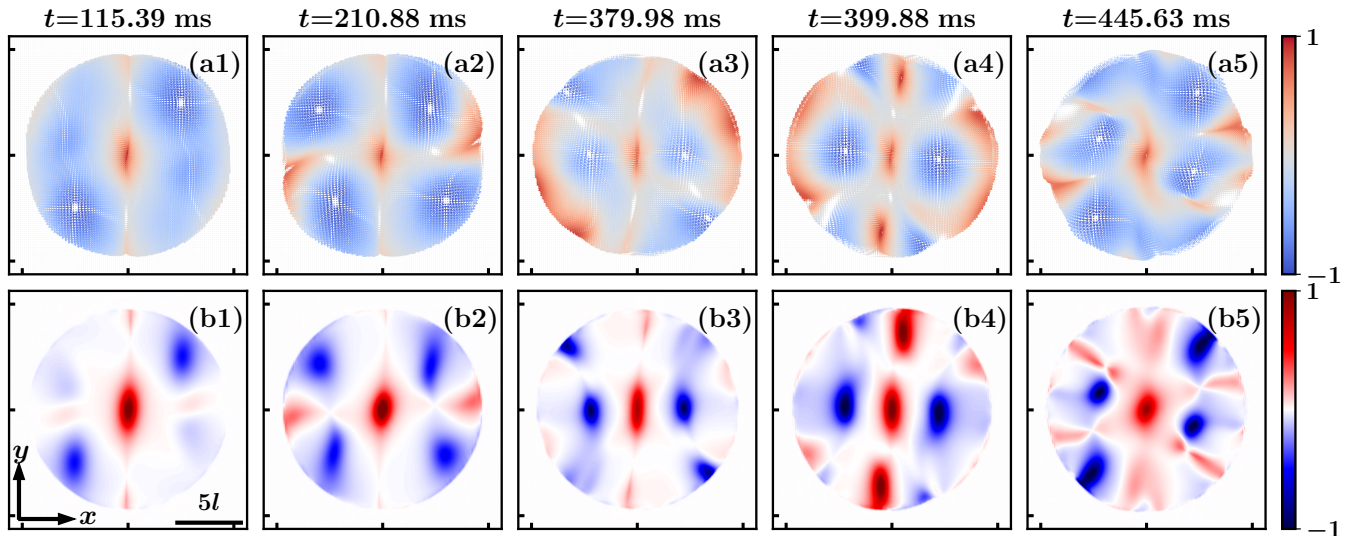


FIG. 4: (a1-a5) shows the evolution of the spin texture \mathbf{S} during the dynamics of the SO-coupled spin-1 BEC with magnetization fixed at $m_z = 0$. The color of the arrows represents the magnitude of S_z . (b1-b5) shows the topological charge densities associated with these spin textures, respectively, at different time instances shown in columns: (1) $t = 115.39$ ms, (2) $t = 210.88$ ms, (3) $t = 379.98$ ms, (4) $t = 399.88$ ms, and (5) $t = 445.63$ ms. All the parameters are the same as the initial state shown in Fig. 1. A full movie of dynamic evolution is presented in the supplementary material.

dependent angular momenta interact, driving the angular oscillation of the skyrmion chain. Although the magnetization is fixed [see inset Fig. 3(d1)], spin-exchange collisions enable particle redistribution within the order parameter, as seen in the component-wise population dynamics in Fig. 3(b). The variations in the canonical contribution L_z^c and the spin-dependent angular momenta L_z^s complement each other, suggesting that the total orbital angular momentum L_z^{tot} still remains nearly constant despite the exchange interactions [Fig. 3(d)].

The constrained evolution of the spin texture and the associated topological charge density (Fig. 4) drives the oscillatory motion of the skyrmion chain around its initial equilibrium position [similar to Fig. 2(a)], mimicking the behavior of a simple harmonic oscillator. The anti-skyrmions in the chain move to their extreme positions along the diagonal, return to equilibrium, and then shift to the opposite extreme. Over time, both the spin texture and topological charge shift diagonally from the initial position at the $y = 0$ line, reaching an extreme at $t = 115.39$ ms [Fig. 4(a1, b1)]. From this position, restoring forces from newly formed skyrmions and anti-skyrmions push the chain back to equilibrium at $t = 210.88$ ms [Fig. 4(a2, b2)], reaching it again at $t = 379.98$ ms [Fig. 4(a3, b3)].

As the chain moves toward the opposite diagonal, temporary skyrmions and anti-skyrmions form and disappear, modifying the spin texture. By $t = 399.88$ ms, new skyrmions attract the anti-skyrmions to the other side [Fig. 4(a4, b4)], helping them reach the extreme position

at $t = 445.63$ ms [Fig. 4(a5, b5)]. The system continues to oscillate as it attempts to restore equilibrium, but chaotic dynamics eventually disrupt the spin texture evolution. Throughout, vortices and antivortices appear temporarily, and the oscillatory behavior of the skyrmion chain is analogous to the dynamics of the linear vortex chain in the spin-1 BEC. A full movie of the skyrmion dynamics and snapshots of the component-wise density profiles are available in the supplementary materials.

In addition to investigating the system's dynamics under Case-I and Case-II, we also analyze several key properties to gain a deeper understanding of the dynamical response of the spinor condensate under a sinusoidally varying magnetic field. In Fig. 3(e), we show the temporal evolution of the spatial average of the spin components \overline{S}_α , where $\alpha = (x, y, z)$, to illustrate the spin alignment and fluctuations within the condensate. The spatial average of the transverse spin components \overline{S}_x and \overline{S}_y remain constant at zero over time, indicating no fluctuations in these directions. However, the spatial average of the longitudinal component \overline{S}_z exhibits dynamic variations due to symmetry breaking in the system. In Case-I, \overline{S}_z fluctuates locally around a mean value, corresponding to the small amplitude oscillations of the skyrmion chain. For Case-II, \overline{S}_z shows more pronounced oscillatory behavior, aligning with the large angular oscillations of the skyrmion chain. This involves creating and annihilating temporary spin structures during the dynamics, contributing to the overall spin texture. In both cases, we examine the scissors mode being excited in the spin texture to

validate the spin fluctuations during the oscillations [69]. We compute $d_{xy} = \langle xyS_z \rangle$ as a function of time and confirm the oscillatory response for both cases as presented in Fig. 3(f). For the free m_z case, the scissors mode oscillates uniformly, but when the system is constrained with longitudinal magnetization $m_z = 0$, the oscillations have non-uniform amplitudes. Further, we examine the spin-spin time correlation given as,

$$C_z(t) = \int \int dt' d\mathbf{r} S_z(\mathbf{r}, t + t') S_z(\mathbf{r}, t') \quad (3)$$

for the dynamics of the initial state prepared with certain fixed m_z . We present the variation of $C_z(t)$ w.r.t time in Fig. 3(g). For Case-I, as the system is not constrained, the time correlation owing to the relaxed dynamics has a supposedly long correlation time. The $C_z(t)$ varies marginally over time, *i.e.*, the spin texture is well time-correlated for this case owing to the bounded changes we observe in the spin texture. However, for Case-II, following the skyrmion chain oscillations, the spin-spin time correlation has an oscillatory response, and as the spin texture gets non-uniform and disturbed over time, the amplitudes of $C_z(t)$ is damped over time. In the supplementary materials, we also discuss the spin-spin space correlations $C_z(\mathbf{r})$ for both cases at various time instances.

In conclusion, we have investigated the unique spin texture dynamics of a spin-orbit-coupled spin-1 BEC under a polarized sinusoidally varying magnetic field. In its ground state, the SO-coupled BEC exhibits a linear chain of topologically protected skyrmions at the saddle points of the magnetic field. The dynamical evolution of the system, initiated with $m_z = 0$ magnetization, has been studied under both freely evolving and fixed magnetization conditions to understand the role of magnetization in the spin texture dynamics. The system experiences the Einstein-de Haas effect during the free dynamical evolution, owing to which there is an exchange between the spin and total orbital momenta. Our numerical simulation shows angular oscillations of the skyrmion chain about the initial configuration (akin to spin Bloch oscillations [70, 71]) for the fixed magnetization evolution. To further investigate the effect of magnetization on the spin texture dynamics, we provide a brief discussion in the supplementary materials, presenting a comparative study of dynamics with different magnetization values for *e.g.* $m_z = \pm 0.1$. Our preliminary study indicates that increasing SOC strength can produce longer linear skyrmion chains, emphasizing the scalability of the system [19]. Further, relevant studies in classical systems [72, 73] and ferrofluids [74] suggest controlled skyrmion formation depending on the strength and periodicity of the magnetic field. Such studies can potentially reveal new insights into skyrmion dynamics and quantum control of ultracold gases with spin degrees of freedom. Spinor BECs thus present a promising platform to study quantum fluid prop-

erties with solid-state parallels, opening new directions for research in complex spinor systems. This work lays a foundation for future exploration into multi-component spinor BECs, especially under varying the SOC strengths and magnetic field parameters.

We thank Jae-yoon Choi and Se Kwon Kim for the insightful and enriching email exchanges. We are indebted to Hari Sadhan Ghosh for his valuable suggestions and Subrata Das for his technical assistance. We acknowledge the National Supercomputing Mission (NSM) for providing the computational resources of PARAM Shakti at IIT Kharagpur, implemented by C-DAC and supported by the Ministry of Electronics and Information Technology (MeitY) and the Department of Science and Technology (DST), Government of India. A.S. gratefully acknowledges support from the Prime Minister's Research Fellowship (PMRF), India. S.H. acknowledges the MHRD, Govt. of India, for the research fellowship.

* arpana.saboo@gmail.com

† sonjoym@phy.iitkgp.ac.in

- [1] D. S. Hall, M. R. Matthews, J. R. Ensher, C. E. Wieman, and E. A. Cornell, *Physical Review Letters* **81**, 4531 (1998).
- [2] D. S. Hall, M. R. Matthews, C. E. Wieman, and E. A. Cornell, *Physical Review Letters* **81**, 1543 (1998).
- [3] M. R. Matthews, D. S. Hall, D. S. Jin, J. R. Ensher, C. E. Wieman, E. A. Cornell, F. Dalfovo, C. Minniti, and S. Stringari, *Physical Review Letters* **81**, 243 (1998).
- [4] T.-L. Ho, *Physical Review Letters* **81**, 742 (1998).
- [5] T. Ohmi and K. Machida, *Journal of the Physical Society of Japan* **67**, 1822 (1998).
- [6] M. Koashi and M. Ueda, *Phys. Rev. Lett.* **84**, 1066 (2000).
- [7] H. Flayac, H. Tercas, D. D. Solnyshkov, and G. Malpuech, *Phys. Rev. B* **88**, 184503 (2013).
- [8] Y. Eto, H. Shibayama, K. Shibata, A. Torii, K. Nabeta, H. Saito, and T. Hirano, *Phys. Rev. Lett.* **122**, 245301 (2019).
- [9] R. M. Kroeze, Y. Guo, V. D. Vaidya, J. Keeling, and B. L. Lev, *Phys. Rev. Lett.* **121**, 163601 (2018).
- [10] M. Scherer, B. Lücke, J. Peise, O. Topic, G. Gebreyesus, F. Deuretzbacher, W. Ertmer, L. Santos, C. Klempt, and J. J. Arlt, *Phys. Rev. A* **88**, 053624 (2013).
- [11] S. Hoshi and H. Saito, *Phys. Rev. A* **81**, 013627 (2010).
- [12] S. Sachdev, *Physics World* **12**, 33 (1999).
- [13] S. Huh, K. Mukherjee, K. Kwon, J. Seo, J. Hur, S. I. Mistakidis, H. Sadeghpour, and J.-y. Choi, *Nature Physics* **20**, 402 (2024).
- [14] S. Huh, W. Yun, G. Yun, S. Hwang, K. Kwon, J. Hur, S. Lee, H. Takeuchi, S. K. Kim, and J. yoon Choi, *Beyond skyrmion spin texture from quantum kelvin-helmholtz instability* (2024), arXiv:2408.11217 [cond-mat.quant-gas].
- [15] S. M. Jose, K. Sah, and R. Nath, *Phys. Rev. A* **108**, 023308 (2023).
- [16] A. Saboo, S. Halder, S. Das, and S. Majumder, *Phys. Rev. A* **108**, 013320 (2023).
- [17] N. Kumar, S. N. Guin, K. Manna, C. Shekhar, and C. Felser, *Chemical Reviews* **121**, 2780 (2021).

- [18] T. Ozawa and H. M. Price, *Nature Reviews Physics* **1**, 349 (2019).
- [19] A. Saboo, S. Halder, S. Das, and S. Majumder, *Phys. Rev. A* **110**, 033325 (2024).
- [20] Y. Eto, H. Shibayama, H. Saito, and T. Hirano, *Phys. Rev. A* **97**, 021602 (2018).
- [21] T. Mithun, R. Carretero-González, E. G. Charalampidis, D. S. Hall, and P. G. Kevrekidis, *Phys. Rev. A* **105**, 053303 (2022).
- [22] Y.-J. Lin, K. Jiménez-García, and I. B. Spielman, *Nature* **471**, 83 (2011).
- [23] C. Wang, C. Gao, C.-M. Jian, and H. Zhai, *Phys. Rev. Lett.* **105**, 160403 (2010).
- [24] H. Hu, B. Ramachandhran, H. Pu, and X.-J. Liu, *Phys. Rev. Lett.* **108**, 010402 (2012).
- [25] P. Wang, Z.-Q. Yu, Z. Fu, J. Miao, L. Huang, S. Chai, H. Zhai, and J. Zhang, *Physical Review Letters* **109**, 095301 (2012).
- [26] B. M. Anderson, G. Juzeliūnas, V. M. Galitski, and I. B. Spielman, *Physical Review Letters* **108**, 235301 (2012).
- [27] Z. Wu, L. Zhang, W. Sun, X.-T. Xu, B.-Z. Wang, S.-C. Ji, Y. Deng, S. Chen, X.-J. Liu, and J.-W. Pan, *Science* **354**, 83 (2016).
- [28] L. Huang, Z. Meng, P. Wang, P. Peng, S.-L. Zhang, L. Chen, D. Li, Q. Zhou, and J. Zhang, *Nature Physics* **12**, 540 (2016).
- [29] D. L. Campbell, G. Juzeliūnas, and I. B. Spielman, *Physical Review A* **84**, 025602 (2011).
- [30] H. Wang, L. Wen, H. Yang, C. Shi, and J. Li, *Journal of Physics B: Atomic, Molecular and Optical Physics* **50**, 155301 (2017).
- [31] J.-G. Wang and Y.-Q. Li, *Results in Physics* **17**, 103099 (2020).
- [32] C.-F. Liu, Y.-M. Yu, S.-C. Gou, and W.-M. Liu, *Physical Review A* **87**, 063630 (2013).
- [33] B. Ramachandhran, B. Opanchuk, X.-J. Liu, H. Pu, P. D. Drummond, and H. Hu, *Physical Review A* **85**, 023606 (2012).
- [34] S. Gautam and S. K. Adhikari, *Phys. Rev. A* **93**, 013630 (2016).
- [35] J.-R. Li, J. Lee, W. Huang, S. Burchesky, B. Shteynas, F. c. Top, A. O. Jamison, and W. Ketterle, *Nature* **543**, 91 (2017).
- [36] L.-C. Zhao, X.-W. Luo, and C. Zhang, *Physical Review A* **101**, 023621 (2020).
- [37] K. T. Geier, G. I. Martone, P. Hauke, W. Ketterle, and S. Stringari, *Phys. Rev. Lett.* **130**, 156001 (2023).
- [38] T. Mithun, A. R. Fritsch, G. N. Koutsokostas, D. J. Frantzeskakis, I. B. Spielman, and P. G. Kevrekidis, *Phys. Rev. A* **109**, 023328 (2024).
- [39] T. Kawakami, T. Mizushima, M. Nitta, and K. Machida, *Physical Review Letters* **109**, 015301 (2012).
- [40] H.-B. Luo, L. Li, and W.-M. Liu, *Scientific Reports* **9**, 18804 (2019).
- [41] S.-W. Su, I.-K. Liu, Y.-C. Tsai, W. M. Liu, and S.-C. Gou, *Physical Review A* **86**, 023601 (2012).
- [42] M. Ueda, *Reports on Progress in Physics* **77**, 122401 (2014).
- [43] S. L. Zhang, W. W. Wang, D. M. Burn, H. Peng, H. Berger, A. Bauer, C. Pfeleiderer, G. van der Laan, and T. Hesjedal, *Nature Communications* **9**, 2115 (2018).
- [44] M. Kato, X.-F. Zhang, D. Sasaki, and H. Saito, *Phys. Rev. A* **94**, 043633 (2016).
- [45] J.-y. Choi, W. J. Kwon, and Y.-i. Shin, *Phys. Rev. Lett.* **108**, 035301 (2012).
- [46] A. Smith, B. Jobst, A. G. Green, and F. Pollmann, *Phys. Rev. Res.* **4**, L022020 (2022).
- [47] C. H. Marrows and K. Zeissler, *Applied Physics Letters* **119**, 250502 (2021).
- [48] T. Chen and T. Byrnes, *Phys. Rev. B* **99**, 184427 (2019).
- [49] G. Kimbell, C. Kim, W. Wu, M. Cuoco, and J. W. A. Robinson, *Communications Materials* **3**, 19 (2022).
- [50] D. Rana, S. Dash, M. Bhakar, R. R. Chowdhury, R. P. Singh, S. Kumar, and G. Sheet, *Phys. Rev. B* **108**, 184419 (2023).
- [51] C.-F. Liu and W. M. Liu, *Phys. Rev. A* **86**, 033602 (2012).
- [52] Y.-K. Liu, N. Yue, J.-J. Zhang, and S.-J. Yang, *Results in Physics* **56**, 107263 (2024).
- [53] Q.-L. Zhu, L. Pan, and J. An, *Phys. Rev. A* **102**, 053320 (2020).
- [54] J.-y. Choi, W. J. Kwon, M. Lee, H. Jeong, K. An, and Y.-i. Shin, *New Journal of Physics* **14**, 053013 (2012).
- [55] Y.-K. Liu and S.-J. Yang, *Chaos, Solitons & Fractals* **132**, 109546 (2020).
- [56] B. M. Anderson, I. B. Spielman, and G. Juzeliūnas, *Physical Review Letters* **111**, 125301 (2013).
- [57] H. Yang, X. Su, Y. Zhang, and L. Wen, *Communications in Theoretical Physics* **74**, 105501 (2022).
- [58] H. Yang, Q. Zhang, and Z. Jian, *Frontiers in Physics* **10**, 910818 (2022).
- [59] Y. Kawaguchi and M. Ueda, *Physics Reports* **520**, 253 (2012).
- [60] In the absence of SOC, the spin-1 BEC under a sinusoidally varying magnetic field has a local high density elongated along the y -axis for the $m_F = \pm 1$ components and fragmented density in the $m_F = 0$ component; although, without any topological excitations in the system.
- [61] T. Mizushima, N. Kobayashi, and K. Machida, *Phys. Rev. A* **70**, 043613 (2004).
- [62] K. Kasamatsu, M. Tsubota, and M. Ueda, *Phys. Rev. A* **71**, 043611 (2005).
- [63] Here onwards, we characterize anti-skyrmions based on the S_z value and the -ve topological charge it carries.
- [64] We calculate the deviation $\Delta A = A - A_{avg}$ for any measurable A . Here, we discuss the variation of ΔL_z^{tot} vs. Δm_z .
- [65] C. Qu and S. Stringari, *Phys. Rev. Lett.* **120**, 183202 (2018).
- [66] S. Li and H. Saito, *Quantum droplets with magnetic vortices in spinor dipolar bose-einstein condensates* (2024), arXiv:2402.18885 [cond-mat.quant-gas].
- [67] F. Y. Lim and W. Bao, *Phys. Rev. E* **78**, 066704 (2008).
- [68] Y. Kawaguchi, H. Saito, and M. Ueda, *Phys. Rev. Lett.* **96**, 080405 (2006).
- [69] C. Qu, C.-H. Li, Y. P. Chen, and S. Stringari, *Phys. Rev. A* **108**, 053316 (2023).
- [70] D. M. Gangardt and A. Kamenev, *Phys. Rev. Lett.* **102**, 070402 (2009).
- [71] Y. V. Kartashov, V. V. Konotop, D. A. Zezyulin, and L. Torner, *Phys. Rev. Lett.* **117**, 215301 (2016).
- [72] H. Du, R. Che, L. Kong, X. Zhao, C. Jin, C. Wang, J. Yang, W. Ning, R. Li, C. Jin, *et al.*, *Nature communications* **6**, 8504 (2015).
- [73] Z. Hou, Q. Zhang, G. Xu, C. Gong, B. Ding, Y. Wang, H. Li, E. Liu, F. Xu, H. Zhang, Y. Yao, G. Wu, X.-x. Zhang, and W. Wang, *Nano Letters* **18**, 1274 (2018).
- [74] S. Koraltan, C. Abert, F. Bruckner, M. Heigl, M. Albrecht, and D. Suess, *Phys. Rev. B* **108**, 134401 (2023).

Supplementary Material for “Magnetization induced skyrmion dynamics of a spin-orbit-coupled spinor condensate under sinusoidally varying magnetic field”

Arpana Saboo,^{1,*} Soumyadeep Halder,¹ Mithun Thudiyangal,² and Sonjoy Majumder^{1,†}

¹*Department of Physics, Indian Institute of Technology Kharagpur, Kharagpur, West Bengal 721302, India*

²*Department of Physics and Electronics, Christ University, Bengaluru, Karnataka 560029, India*

SM1. DETAILS OF NUMERICAL SIMULATIONS

We cast the system in a Quasi-2D form by considering a Gaussian ansatz along the axial direction, thereby integrating it out. The Quasi-2D dimensionless Gross-Pitaevskii equations (GPEs) governing the dynamics of the spin-1 system reads as,

$$i\partial_t\psi_{\pm 1} = \left[-\frac{1}{2}\nabla^2 + V + c_0|\psi|^2 + c_2(\pm|\psi_1|^2 + |\psi_0|^2 \mp |\psi_{-1}|^2) \right] \psi_{\pm 1} + c_2\psi_{\mp 1}^*\psi_0^2 - i\gamma(\partial_y \pm i\partial_x)\psi_0 + B_0 \sin x\psi_0 \quad (\text{S1})$$

$$i\partial_t\psi_0 = \left[-\frac{1}{2}\nabla^2 + V + c_0|\psi|^2 + c_2(|\psi_1|^2 + |\psi_{-1}|^2) \right] \psi_0 + 2c_2\psi_1\psi_0^*\psi_{-1} - i\gamma(\partial_y - i\partial_x)\psi_1 - i\gamma(\partial_y + i\partial_x)\psi_{-1} + B_0 \sin x(\psi_1 + \psi_{-1}) \quad (\text{S2})$$

where $\psi_{m_F} = N^{-1/2}l\Psi_{m_F}$ ($m_F = \pm 1, 0$) denotes the dimensionless m_F -th component wave function and $|\psi|^2 = \sum_{m_F} |\psi_{m_F}|^2$ is the total particle density confined in dimensionless external potential $V = (x^2 + y^2)/2$. The contact interaction parameters in the dimensionless form are given as $c_0 = 2N\sqrt{2\pi\lambda}(a_0 + 2a_2)/3l$ and $c_2 = 2N\sqrt{2\pi\lambda}(a_2 - a_0)/3l$, respectively. In our numerical calculations, the lengths, time, energy (interaction and SOC), and magnetic field are measured in the units of $l, 1/\omega_{\perp}, \hbar\omega_{\perp}$ and $(g_F\mu_B l)/\hbar\omega_{\perp}$, respectively. We use the split-step Crank-Nicolson scheme [S1–S3] to numerically solve the GPEs (S1–S2) for imaginary time propagation to generate the ground state solutions and for real-time propagation to study the dynamical evolution. In our simulations, we have considered 10^4 number of ^{87}Rb atoms confined in a quasi-2D harmonic trap V with transverse trapping frequency, $\omega_{\perp} = 2\pi \times 20$ Hz with trap aspect ratio, $\lambda = \omega_z/\omega_{\perp} = 20$ and the characteristic oscillator length, $l = 2.41\mu\text{m}$. The s -wave scattering lengths for channels of total spin 0 and 2 are $a_0 = 101.8a_B$ and $a_2 = 100.4a_B$, respectively, where a_B is the Bohr radius. We keep the magnetic field strength $B_0 = 0.25$ and the SOC strength $\gamma = 0.5$. Our simulations run from a spatial extent of $-20l$ to $20l$ in both x and y directions with 2001×2001 grid points. The employed spatial discretization refers to $\Delta x = \Delta y = 0.02l$, with a time step $\delta t = (2 \times 10^{-4})/\omega_{\perp}$.

SM2. GROUND STATE IN THE ABSENCE OF SPIN-ORBIT COUPLING

We here discuss the ground state solution of the spin-1 BEC under the influence of the sinusoidally varying magnetic field, in the absence of SOC. The x -polarised sinusoidal magnetic field affects the spin-exchange interaction, as confirmed by the coupled GPEs (S1–S2) of the main text. We present the ground state densities of the spin-1 order parameter in Fig. S1. In the absence of SOC, the system’s symmetry is preserved, and the overall angular momentum

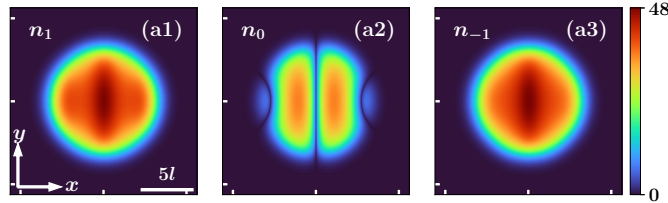


FIG. S1: (a1–a3) shows the ground state density profiles n_1 , n_0 and n_{-1} of $m_F = 1, 0, -1$ components respectively of a ferromagnetic spin-1 BEC of 10^4 ^{87}Rb atoms in a sinusoidally varying magnetic field $B(\mathbf{r}) = (B_0 \sin x, 0)$ in the absence of SOC. The scattering length $a_0 = 101.8a_B$ and $a_2 = 100.4a_B$. The spin-1 BEC is confined in an axisymmetric trap with $(\omega_{\perp}, \omega_z) = 2\pi \times (20, 400)\text{Hz}$. The units of length is $\sqrt{\hbar/M\omega_{\perp}}$.

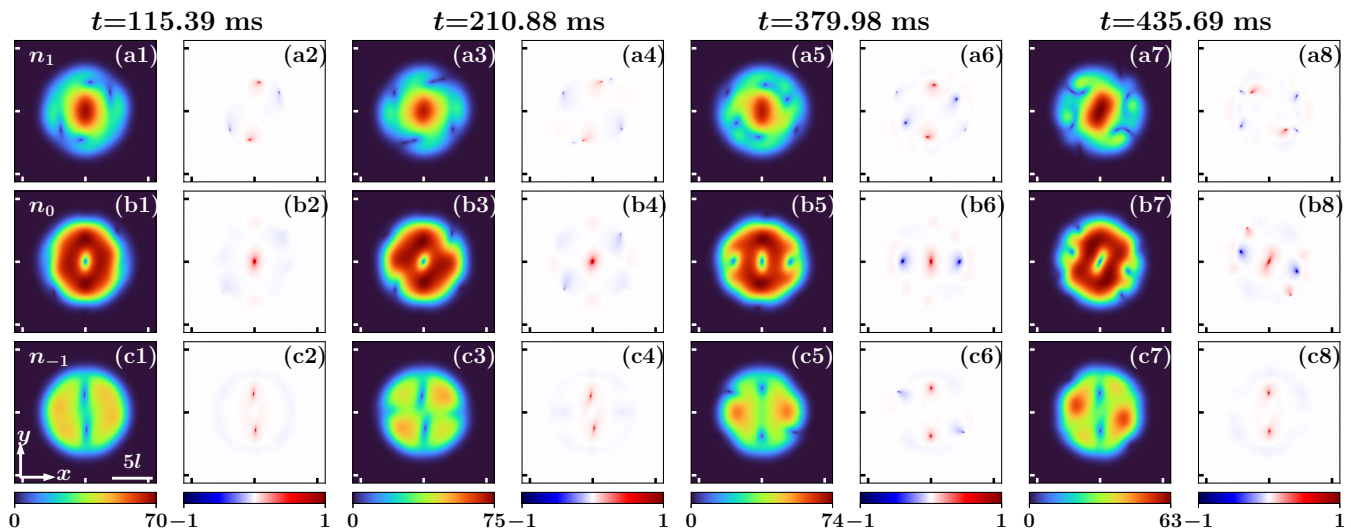


FIG. S2: The component-wise density profiles n_1 , n_0 and n_{-1} and their corresponding vorticity profiles are shown in alternate columns for different time instances. Column 1 (a1, b1, c1) and column 2 (a2, b2, c2) shows the densities and vortices, respectively at $t = 115.39$ ms, column 3 (a3, b3, c3) and column 4 (a4, b4, c4) show the same at $t = 210.88$ ms, column 5 (a5, b5, c5) and column 6 (a6, b6, c6) for $t = 379.98$ ms and column 7 (a7, b7, c7) and column 8 (a8, b8, c8) for $t = 435.69$ ms. All parameters are the same as for the initial state shown in Fig. 1 of the main text.

remains conserved. However, the sinusoidal magnetic field renders fragments in the density profile of the $m_F = 0$ component. As the saddle points of the sinusoidal magnetic field occur at multiples of π , the fragment lines pass through $x = 0, \pm\pi$. The $m_F = \pm 1$ components have a region of relatively higher density located about the $x = 0$ line.

SM3. DYNAMICS OF THE SO-COUPLED SPIN-1 BEC

We present here the dynamical evolution of the ground state densities of the SO-coupled spin-1 BEC. In the main text, we discussed the spin texture dynamics under two cases of magnetization. For freely evolving magnetization, as the system has an effectively stronger spin-spin time correlation, the density profiles for the $m_F = 0, \pm 1$ vary minimally during the dynamics. However, for the case with magnetization constrained at $m_z = 0$ during the dynamics, the densities vary in accordance with the associated spin texture dynamics, with adjuvant creation and annihilation of vortices in the system. The snapshots of density and vorticity profiles at various time instances are shown in Fig. S2. The vortex chain engendered in the $m_F = 0$ component due to the synergistic interaction of the magnetic field and the SOC, starts to disorient from the initial position and at about time $t = 115.39$ ms, aligns along the diagonal (see the first two columns of Fig. S2). The anti-vortices in the $m_F = 1, 0$ components gradually move towards the periphery of the system, while for the $m_F = -1$ component, the density lobes are oriented along the extremum. Thereafter, the system tries to restore back to its equilibrium. To facilitate this, density modulation along the opposite diagonal is observed at about time $t = 210.88$ ms (see third and fourth columns of Fig. S2), and eventually at time $t = 379.98$ ms, the system is restored back to the equilibrium as shown in the fifth and sixth columns of Fig. S2. The vortex chain then continues to move further towards the other extremum and orients along the other diagonal at about $t = 445.63$ ms as shown in the last two columns. The system, thus, exhibits an oscillatory response during the dynamics as confirmed by the skyrmion dynamics.

SM4. SPIN-SPIN CORRELATIONS

We analyze the spin-spin space correlation for the z -component of the spin texture during the dynamics under both cases of magnetization. At any time instant, t , the space correlation is defined as [S4–S7],

$$C_z(\mathbf{r}, t) = \int d\mathbf{r}' S_z(\mathbf{r} + \mathbf{r}', t) S_z(\mathbf{r}, t) \quad (\text{S3})$$

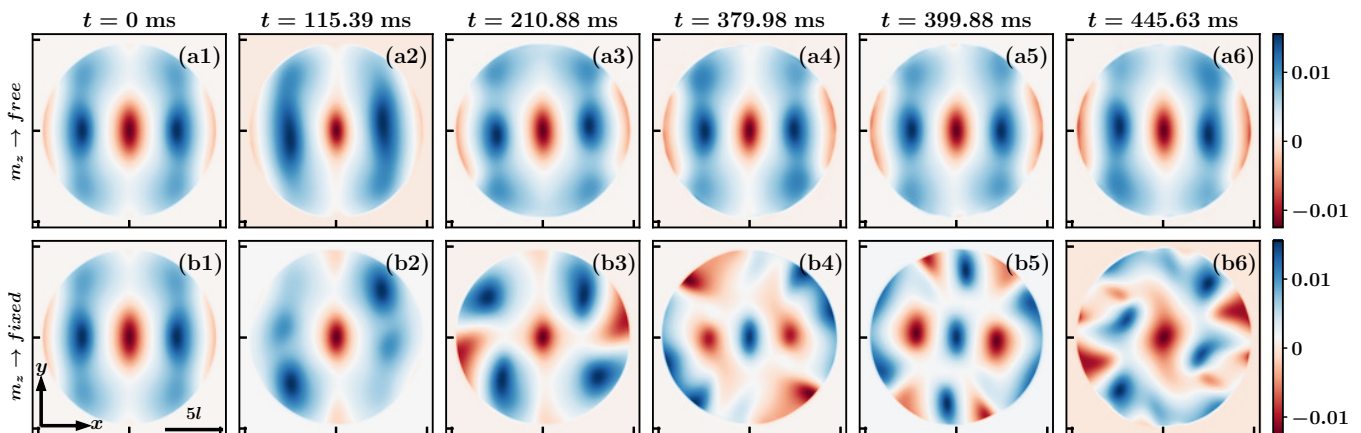


FIG. S3: (a1-a6) demonstrates the spin-spin space correlations in S_z for various time instances during the dynamical evolution of the system under the free m_z case. (b1-b6) represent the same for the fixed m_z case. All parameters are the same as for the initial state shown in Fig. 1 of the main text.

We present the space correlations for both cases at various time instances in Fig. S3. The top panel shows the $C_z(\mathbf{r}, t)$ distributions for the free magnetization case, and the bottom panel represents the same for the constrained evolution. At the initial time, $t = 0$ ms, the correlation distribution mimics a sinusoidal function along the x -axis. During the dynamics, the distribution depicts the dynamical response of the spin texture. In the case of freely evolving magnetization, the system remains very strongly correlated over time owing to the marginal changes in the spin texture. However, the constrained magnetization case reveals an oscillatory response leading to the formation of certain temporary domains in the distribution. These domains also affirm the spin vortices and their evolution with time.

SM5. DEPENDENCE ON MAGNETIZATION VALUES

In this section, we explore different cases for various magnetization values and study the dynamics of the prepared states. From the ground state solutions of the GPEs, the system naturally settles at a magnetization value of $m_z = -0.07$. The dynamical evolution of this state under free magnetization dynamics reveals steady-state behavior. The population variation is presented in Fig. S4(a), showing that the particle number in each m_F component remains constant in the steady state. Additionally, both the orbital and spin angular momenta are conserved quantities, as indicated in Fig. S4(b). Consequently, the system exhibits the Einstein-de Haas effect [see Fig. S4 (b1)]. The steady-state dynamics confirm no significant variation in the spin texture, leading to a constant time correlation [see Fig. S4 (c)].

We further study the dynamics of the system prepared with magnetization $m_z = \mp 0.1$ and draw comparisons from the steady state. As $m_z = -0.1$ is pretty close to the steady state, the dynamic behavior of this state can be analogously understood. During the free magnetization evolution, the system experiences an oscillatory population variation [see Fig. S4 (d)] due to the allowed particle exchange during the spin-mixing dynamics. This is also reflected in the oscillatory m_z variation, which complements the L_z variation, indicating the possibility of orbital and spin angular momentum exchanges as shown in Fig. S4 (e). The Einstein-de Haas effect (Fig. S4 (e1)) testifies for this angular momentum exchange. As this system is slightly deviated from the steady state, the spin texture, S_z in particular shows slight variation with time and thus its time correlation C_z as shown in Fig. S4 (f). For $m_z = 0.1$, the dynamical evolution is slightly offset (as the state is far from the steady state), as confirmed by the population variation shown in Fig. S4 (g). The L_z and m_z variations are more pronounced [see Fig. S4 (h)], which leads to slight variation in the total angular momentum of the system [inset Fig. S4 (h1)]. During the free magnetization evolution, the spin texture and the correlation in S_z show significant variations as presented in Fig. S4 (i).

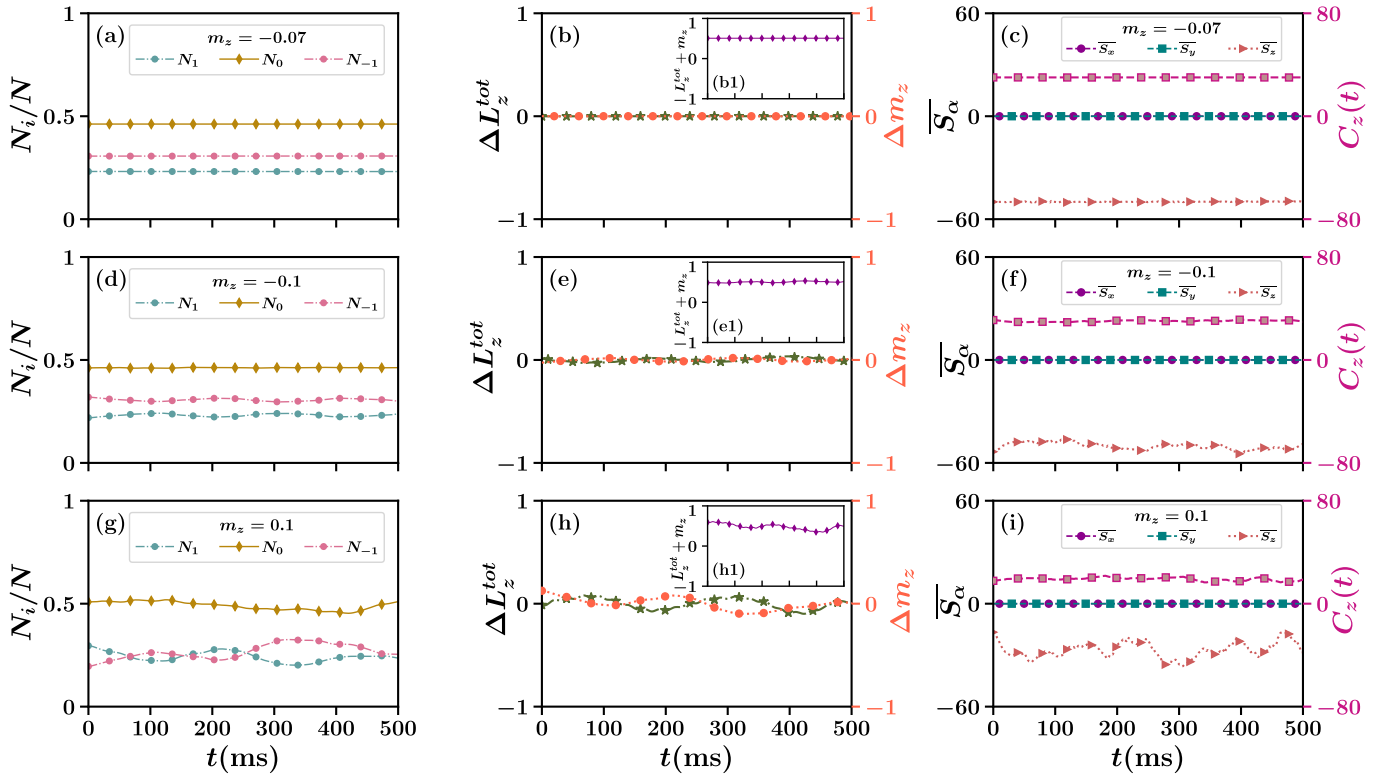


FIG. S4: The top panel represents (a) population variation; (b) ΔL_z^{tot} and Δm_z variation with total angular momentum variation in inset (b1); spin texture S_α and time correlation $C_z(t)$ variation for the ground state prepared with free magnetization ($m_z = -0.07$) following a free magnetization dynamics. The middle and bottom panels represent the same for the states prepared with fixed magnetization $m_z = \mp 0.1$, respectively.

Thus, longitudinal magnetization m_z plays a pivotal role in leading the system from a well-correlated state to one with noticeable differences.

* arpana.saboo@gmail.com

† sonjoym@phy.iitkgp.ac.in

- [S1] J. Crank and P. Nicolson, *Mathematical Proceedings of the Cambridge Philosophical Society* **43**, 10.1017/S0305004100023197 (1947).
- [S2] X. Antoine, W. Bao, and C. Besse, *Computer Physics Communications* **184**, 2621 (2013).
- [S3] P. Muruganandam and S. K. Adhikari, *Computer Physics Communications* **180**, 1888 (2009).
- [S4] H. Saito, Y. Kawaguchi, and M. Ueda, *Phys. Rev. A* **76**, 043613 (2007).
- [S5] L. A. Williamson and P. B. Blakie, *Phys. Rev. Lett.* **116**, 025301 (2016).
- [S6] S. M. Jose, K. Sah, and R. Nath, *Phys. Rev. A* **108**, 023308 (2023).
- [S7] S. Huh, K. Mukherjee, K. Kwon, J. Seo, J. Hur, S. I. Mistakidis, H. Sadeghpour, and J.-y. Choi, *Nature Physics* **20**, 402 (2024).